Numerical simulation of droplet evaporation between two circular plates [†]

Hangjin Ban and Gihun Son[*]

Department of Mechanical Engineering, Sogang University, 35 Baekboem-ro, Mapo-gu, Seoul, 121-742, Korea

---

Abstract

Numerical simulation is performed for droplet evaporation between two circular plates. The flow and thermal characteristics of the droplet evaporation are numerically investigated by solving the conservation equations of mass, momentum, energy and mass fraction in the liquid and gas phases. The liquid-gas interface is tracked by a sharp-interface level-set method which is modified to include the effects of evaporation at the liquid-gas interface and contact angle hysteresis at the liquid-gas-solid contact line. An analytical model to predict the droplet evaporation is also developed by simplifying the mass and vapor fraction equations in the gas phase. The numerical results demonstrate that the 1-D analytical prediction is not applicable to the high rate evaporation process. The effects of plate gap and receding contact angle on the droplet evaporation are also quantified.

Keywords: Contact angle hysteresis; Droplet evaporation; Level-set method; Mass transfer

---

1. Introduction

Droplet evaporation on a solid surface has received significant attention as an efficient fabrication process for various microstructures [1-4]. Despite extensive experimental and theoretical studies of evaporation process [4-6], its general predictive model has not yet been developed due to the complexity of the interfacial flow including heat transfer, mass transfer, phase change and contact line dynamics.

Recently, as a more simplified and easily controllable process, the evaporation of a liquid droplet in the confined geometry between two circular transparent plates was investigated by Clément and Leng [7]. They obtained 2-dimensional (or 1-dimensional axisymmetric in the ideal case) images of the temporal evolution of an evaporating droplet in confined geometry and compared theoretical prediction based on the 1-dimensional diffusion equation of vapor number density with measured droplet contact area. Subsequently, the confined geometry was employed by Leng [8] for the evaporation of a hard-sphere colloidal suspension. Although the evaporation process is expected to be well defined and easily controllable in the confined geometry, it is not clear that the characteristics of flow, heat and mass transfer are negligible across the film thickness normal to the plates considering no-slip and contact angle condition on the plates.

Numerical simulations for general analysis of droplet evaporation were performed in several studies using a finite element method (FEM) [10, 11] and a body-fitted moving-grid method [12]. The Lagrangian methods generally are not easy to handle breaking of the interface. Such difficulties can be overcome with Eulerian interface tracking methods such as the volume-of-fluid (VOF) method and a level-set (LS) method.

Briones et al. [13] computed droplet impact and evaporation using the explicit VOF method in the commercial CFD code FLUENT. However, the coupled interface conditions for the vapor concentration, temperature and evaporation flux are not easy to implement in the VOF method.

Tangui et al. [14] developed the LS method for computation of droplet evaporation combining with the ghost fluid approach to accurately implement the interface conditions. Subsequently, Son [15, 16] developed the LS method for droplet impact and evaporation on a solid surface by employing an iterative calculation procedure for the coupled interface conditions for the temperature and vapor fraction.

In this study, the LS method is further developed for simulations of droplet evaporation between two circular plates and validation test of its theoretical prediction. The effects of plate gap and receding contact angle on the droplet evaporation are investigated.

2. Numerical analysis

The present numerical approach is based on the sharp-interface LS formulation developed by Son [15, 16] for droplet evaporation on a solid surface. The LS method is extended

---

[*]Corresponding author. Tel.: +82 2 705 8641, Fax.: +82 2 712 0799
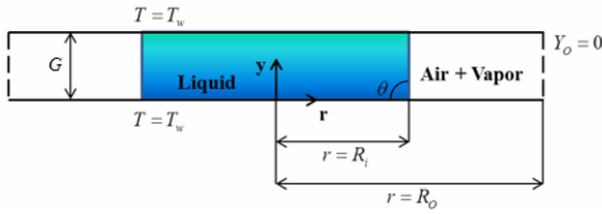E-mail address: gihun@sogang.ac.kr

Fig. 1. Configuration for analysis of liquid droplet evaporation between two circular plates.

for droplet evaporation between two circular plates, as depicted in Fig. 1. The liquid-gas interface is tracked by the LS function ϕ, which is defined as a signed distance from the interface. The negative sign is chosen for the gas phase and the positive sign for the liquid phase. We assume here that the gas is an ideal mixture of air and vapor, while the liquid is a pure substance and the interface temperature is below the boiling temperature.

2.1 Governing equation

The conservation equations of mass, momentum, energy, and the vapor mass fraction Y for the liquid-gas region are expressed as follows [15, 16]:

$$\nabla \cdot \mathbf{u} = v_{lg} \dot{m} \mathbf{n} \cdot \nabla H \tag{1}$$

$$\hat{\rho}(\frac{\partial \mathbf{u}}{\partial t} + \mathbf{u}_f \cdot \nabla \mathbf{u}_f) = -[\nabla p + (\sigma \kappa - v_{lg}\dot{m}^2)\nabla H]$$
$$+ \nabla \cdot \hat{\mu}[\nabla \mathbf{u} - v_{lg}\dot{m}\mathbf{n}\nabla H + (\nabla \mathbf{u}_f)^T] \tag{2}$$

$$\rho_f c_f(\frac{\partial T_f}{\partial t} + \mathbf{u}_f \cdot \nabla T_f) = \nabla \cdot k_f \nabla T_f \quad \text{if } \phi \neq 0;$$
$$T_f = T_{int} \quad \text{if } \phi = 0 \tag{3}$$

$$\rho_g(\frac{\partial Y}{\partial t} + \mathbf{u}_g \cdot \nabla Y) = \nabla \cdot \rho_g \hat{D} \nabla Y \quad \text{if } \phi < 0;$$
$$Y = Y_{int} \quad \text{if } \phi = 0 \tag{4}$$

where

$$H = 1 \text{ if } \phi > 0; \quad H = 0 \text{ if } \phi \leq 0 \tag{5}$$

$$\mathbf{n} = \nabla \phi / |\nabla \phi|; \quad \kappa = \nabla \cdot n \tag{6}$$

$$\mathbf{u}_l = \mathbf{u} + v_{lg}\dot{m}\mathbf{n}(1-H); \quad \mathbf{u}_g = \mathbf{u} + v_{lg}\dot{m}\mathbf{n}H \tag{7}$$

$$\hat{\rho} = \rho_g(1-F) + \rho_l F; \quad \hat{\mu}^{-1} = \mu_g^{-1}(1-F) + \mu_l^{-1}F \tag{8}$$

$$\hat{k}^{-1} = k_g^{-1}(1-F) + k_l^{-1}F \tag{9}$$

$$\hat{D}^{-1} = D_g^{-1}(1-F) \tag{10}$$

$$Y_{int} = \frac{M_v p_{v,sat}(T_{int})}{M_v p_{v,sat}(T_{int}) + M_a[p_\infty - p_{v,sat}(T_{int})]} \tag{11}$$

$$\dot{m} = \mathbf{n} \cdot \rho_g D_g \nabla Y / (1 - Y_{int}) = \frac{\mathbf{n} \cdot (k_l \nabla T_l - k_g \nabla T_g)}{h_{lg}}. \tag{12}$$

Here, the subscript f denotes the liquid phase (l) for $\phi > 0$

and the gas phase (g) for $\phi \leq 0$, and H is the discontinuous step function. The velocity $\mathbf{u}_f$ ($\mathbf{u}_l$ or $\mathbf{u}_g$) for each phase is extrapolated into the entire domain (or a narrow band near the interface) by using the velocity jump condition, $\mathbf{u}_l - \mathbf{u}_g = v_{lg}\dot{m}\mathbf{n} \cdot \nabla H$. The effective properties, ($\hat{\rho}$, $\hat{\mu}$, and $\hat{D}$), are evaluated from a fraction function F, which is described in Ref. [17]. In Eqs. (11) and (12), Y_{int}, T_{int}, and $\dot{m}$ are simultaneously solved using a Newton-Raphson iterative algorithm for their stable calculation [15]. Note that the formulation for energy conservation, given by Eq. (3), is different from that in Refs. [15, 16]. The energy equation for the liquid and gas phases with a source term for the latent heat of vaporization is re-formulated as the energy equation for each phase with the saturation temperature at the interface as a Dirichlet boundary condition. The interface temperature is obtained from Eq. (12) with the latent heat of vaporization. This formulation is much more efficient to implement without changing the numerical results.

2.2 Level-set equations

In the LS formulation, the interface is described as $\phi = 0$. The zero level set of ϕ is advanced as

$$\frac{\partial \phi}{\partial t} + \mathbf{U} \cdot \nabla \phi = 0 \tag{13}$$

where the interface velocity $\mathbf{U}$ is expressed as $\mathbf{U} = \mathbf{u} + \dot{m}\mathbf{n} / \rho_f$. The LS function is reinitialized to a distance function from the interface by obtaining a steady-state solution of the equation.

$$\frac{\partial \phi}{\partial \tau_0} = S(\phi)(1 - |\nabla \phi|) \tag{14}$$

$$S(\phi) = 0 \qquad \text{if } |\phi| \leq h/2$$
$$= \frac{\phi}{\sqrt{\phi^2 + h^2}} \qquad \text{otherwise }. \tag{15}$$

Here h is grid spacing and the formulation of sign function S implies that a near-zero level set rather than ϕ is used as the immobile boundary condition during the reinitialization procedure.

2.3 Boundary conditions

The boundary conditions used in this study are as follows (Refer to Fig. 1).
At the bottom and top walls ($y = 0$, $y = G$),

$$\mathbf{u} = 0, \quad T = T_w, \quad \frac{\partial Y}{\partial y} = 0, \quad \frac{\partial \phi}{\partial y} = \mp \cos \theta. \tag{16}$$

At the symmetry boundary ($r = 0$)

$$\mathbf{u} = 0, \quad \frac{\partial \mathbf{u}}{\partial r} = \frac{\partial T}{\partial r} = \frac{\partial Y}{\partial r} = \frac{\partial \phi}{\partial r} = 0 . \tag{17}$$

At the right boundary ($r = R_0$)

$$\frac{\partial \mathbf{u}}{\partial r} = \frac{\partial T}{\partial r} = \frac{\partial \phi}{\partial r} = 0, \quad p = 0, \quad Y = Y_0 . \tag{18}$$

3. Results and discussion

The computations of droplet evaporation between two circular plates are conducted using the water and air properties at 1atm:

$$\rho_l = 997 kg / m^3 , \qquad \rho_g = 1.18 kg / m^3$$

$$\mu_l = 8.91 \times 10^{-4} Pa \cdot s , \quad \mu_g = 1.85 \times 10^{-5} Pa \cdot s$$

$$c_l = 4.18 \times 10^3 J / kg \cdot K , \quad c_g = 1.01 \times 10^3 J / kg \cdot K$$

$$k_l = 0.595 W / mK , \qquad k_g = 2.55 \times 10^{-2} W / mK$$

$$D_g = 2.6 \times 10^{-5} m^2 / s , \quad \sigma = 7.2 \times 10^{-2} N / m .$$

The saturated-vapor pressure is evaluated as a function of temperature from the steam table [19].

$$p_{v,sat} = \exp\left(9.487 - \frac{3.893 \times 10^3}{T_{int} + 230.47} \right), \tag{19}$$

where $p_{v,sat}$ is given in *MPa* and T_{int} in $^\circ C$. We vary parametrically the receding contact angle θ_r and the gap *G* of two circular plates while keeping the advancing contact angle $\theta_a = 90^\circ$, the wall temperature as $T_w = 90^\circ C$ and the initial temperature as $T_i = 25^\circ C$, the vapor mass fraction at the right side boundary as $Y_o = 0$, and the plate radius as $R_0 = 128 \mu m$, the initial contact radius of droplet as $R_i = 64 \mu m$.

A convergence test for grid resolutions is conducted with $\theta_r = 80^\circ$, G = 32 μm and four different grid spacings of h = 4 μm , h = 2 μm , h = 1 μm , and h = 0.5 μm . The temporal variations of liquid droplet contact radius are plotted in Fig. 2.

The droplet contact radius decreases with evaporation. A small peak is observed during the late period of droplet evaporation when the liquid droplet between two plates is split into two single droplets. The split and elongated droplets are quickly deformed to have a spherical-cap shape due to the surface tension minimizing the interface area, as depicted in Fig. 3. This results in the sharp increase of droplet contact radius. Thereafter, the droplet contact radius decreases again.

The evaporation time for h = 4 μm , h = 2 μm , h = 1 μm , and h = 0.5 μm is $\tau_e = 0.209 s$, $\tau_e = 0.184 s$, $\tau_e = 0.172 s$, and $\tau_e = 0.166 s$, respectively. The relative difference of the computed results between successive mesh sizes is observed to be small as the mesh size decreases. Therefore, most of computations in this study are done with h = 1 μm to save computing time without losing the accuracy of the numerical results.
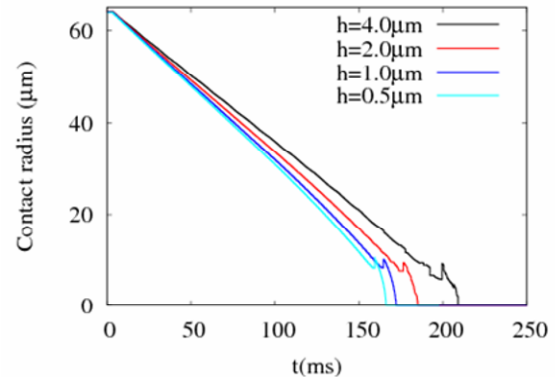

Fig. 2. Effect of mesh size on the temporal variation of the liquid droplet-plate contact radius for $\theta_r = 80^\circ$ and G = 32 μm .
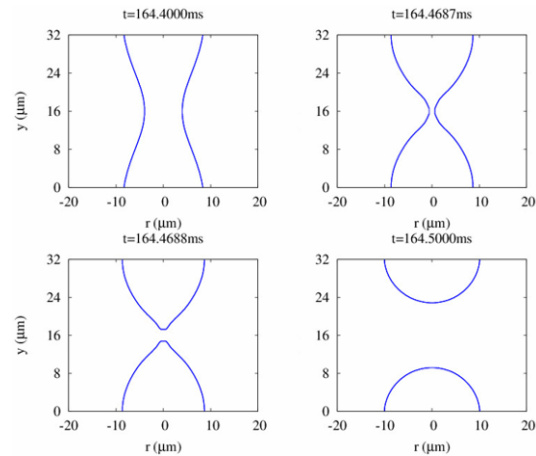

Fig. 3. Evolution of the liquid-gas interface for $\theta_r = 80^\circ$ and G = 32 μm during the late period of droplet evaporation.

3.1 Comparison with theoretical prediction

Computations are carried out to validate the assumptions used by Clément and Leng [7] for the theoretical analysis for liquid droplet evaporation between two circular plates. Assuming that the vapor fraction field is 1-dimensional axisymmetric, the vapor fraction equation is expressed as

$$\frac{\partial Y}{\partial t} + u \frac{\partial Y}{\partial r} = D_g \frac{1}{r} \frac{\partial}{\partial r} r \frac{\partial Y}{\partial r} \qquad \text{if} \quad r > R . \tag{20}$$

The interface velocity is determined as

$$\frac{\partial R}{\partial t} = \frac{\rho_g D_g}{\rho_l (1 - Y_{int})} \left(\frac{\partial Y}{\partial r} \right)_{r=R} . \tag{21}$$

Neglecting the transient and convection terms and assuming the constant interface temperature in Eq. (20), we have

$$\ln\left(\frac{R}{R_o}\right) \frac{\partial R^2}{\partial t} = \frac{2 \rho_g D_g (Y_{int} - Y_o)}{\rho_l (1 - Y_{int})} . \tag{22}$$
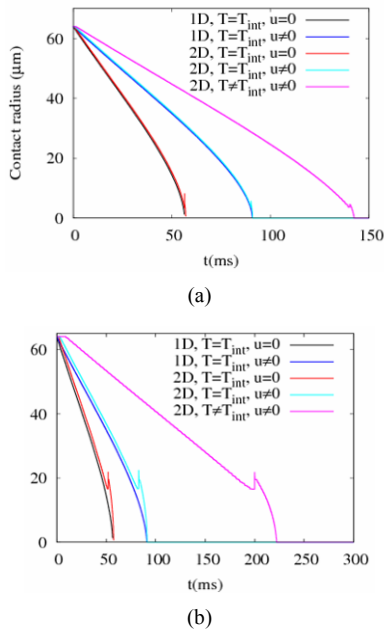
(a)

(b)

Fig. 4. Effect of plate gap on the temporal variation of liquid droplet radius with different conditions for $\theta_r = 80°$: (a) $G = 16\,\mu m$ and; (b) $G = 64\,\mu m$.

Assuming that the interface temperature is constant as $T = T_{int}$ and including convection term as $u \neq 0$, we obtain

$$u = -\frac{\rho_l - \rho_g}{\rho_l}\frac{R}{r}\frac{dR}{dt} \,, \qquad \frac{dR}{dt} = \frac{\rho_g D_g}{\rho_l(1 - Y_{int})}\left(\frac{\partial Y}{\partial r}\right)_{r=R} . \qquad (23)$$

The 1-D moving boundary problem can be easily solved using the following coordinate transformation

$$\xi = r - R \,. \qquad (24)$$

Eq. (20) is transformed as

$$\frac{\partial Y}{\partial t} + (u - \frac{dR}{dt})\frac{\partial Y}{\partial r} = \frac{1}{r}\frac{\partial}{\partial r}D_g r\frac{\partial Y}{\partial r} \quad \text{if } \xi > 1 . \qquad (25)$$

The transformed equations are straightforward to discretize and solve.

In Fig. 4, 1-dimensional theoretical predictions are compared with the numerical results for different plate gaps. The 1-dimensional predictions show a good agreement with the numerical results obtained without/with the transient and convection terms ($u = 0$) as long as no heat transfer ($T = T_{int}$) is assumed. When including the effect of heat transfer, however, the numerical prediction of evaporation time is much longer than the 1-dimensional predictions. The evaporation time increases with the plate gap as $\tau_e \sim G^{0.322}$, which is estimated from the least square fitting from the numerical results.
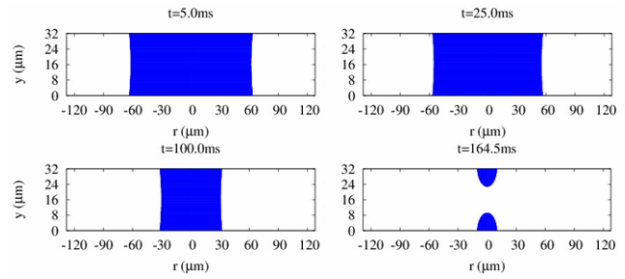

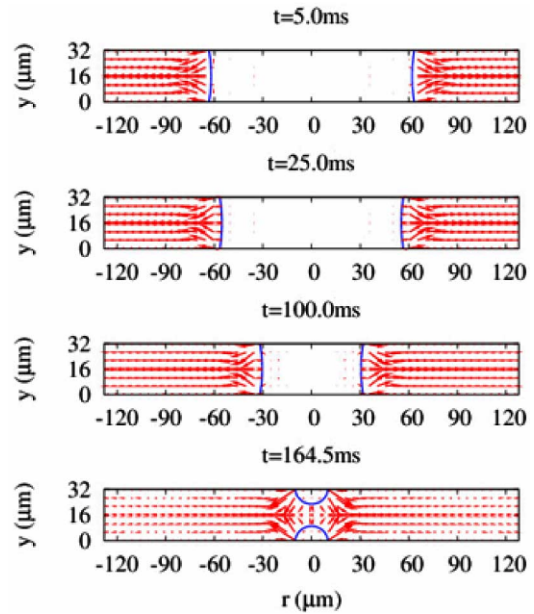Fig. 5. Evolution of an evaporating liquid-gas interface for $\theta_r = 80°$ and $G = 32\,\mu m$.

Fig. 6. Velocity field for $\theta_r = 80°$ and $G = 32\,\mu m$.

3.2 Interfacial motion and the associated flow, temperature and vapor fraction fields

Fig. 5 shows the evolution of an evaporating liquid-gas interface for $\theta_r = 80°$ and $G = 32\,\mu m$. The interface is deformed as the liquid volume decreases with evaporation. The contact line is pinned while the contact angle reaches the receding contact angle of $\theta_r = 80°$ and then the contact line begins to move as seen at $t = 5\,ms$. The liquid film is broken into two droplets at $t = 164.5\,ms$ without any satellite droplets. The velocity, temperature and vapor fraction fields associated with the droplet evaporation are plotted in Figs. 6-8. The liquid phase is almost stationary, whereas the gas velocity is pronounced near the interface. The gas velocity, which is normal to the interface, becomes parallel to the plates away from the interface. The temperature in the liquid-gas phases initially increases due to the heat transfer from the plates and then the temperature field becomes quite uniform except the interface region, where the thermal energy is used for the liquid-vapor phase change. The isothermal pattern near the interface maintains as long as the remaining portion of liquid drop-
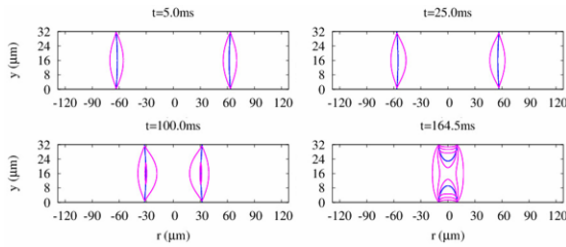
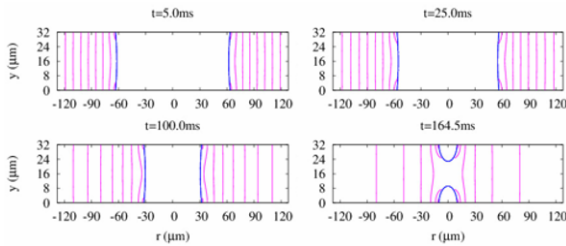Fig. 7. Temperature field for $\theta_r = 80°$ and $G = 32\,\mu m$. The interval between temperature contours is $5°C$.

Fig. 8. Vapor mass fraction field for $\theta_r = 80°$ and $G = 32\,\mu m$. The interval between vapor mass fraction contours is 0.05.

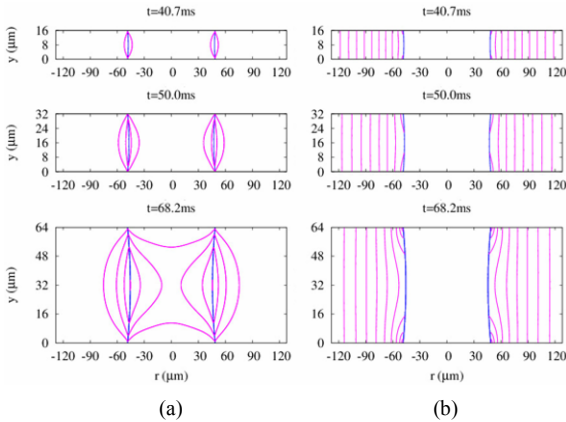Fig. 9. Effect of plate gap on the liquid droplet evaporation for $G = 32\,\mu m$: (a) temperature field; (b) vapor mass fraction. The intervals between temperature and vapor mass fraction contours are $5°C$ and 0.05, respectively.

Fig. 10. Effect of plate gap on temporal variation of liquid droplet-plate contact radius for $\theta_r = 80°$.

Fig. 11. Effect of receding contact angle on the evolution of an evaporating liquid-gas interface: (a) $\theta_r = 30°$; (b) $\theta_r = 80°$.

Fig. 12. Effect of receding contact angle on temporal variation of liquid droplet-plate contact radius for $G = 32\,\mu m$.

let is not so small, as seen at $t = 100.0\,ms$ of Fig. 7. The temperature is not uniform along the interface, which results in the non-uniform vapor fraction distribution, as depicted in Fig. 8. However, the vapor fraction distribution is almost 1-dimensional except the interface.

3.3 Effect of the gap between two plates

The effect of plate gap G on the temperature and vapor fraction field is shown in Fig. 9 while keeping $\theta_r = 80°$. As the gap increases, the temperature field varies in a wider region and the interface temperature become lower in the central region of $y = G/2$. The evaporation rate becomes non-unif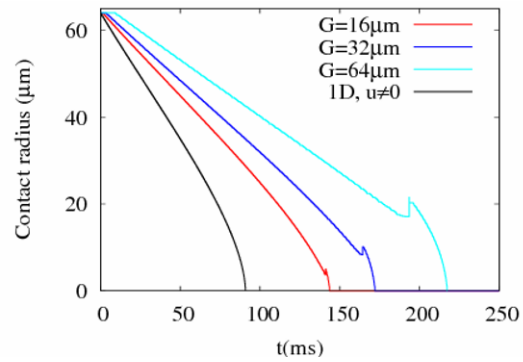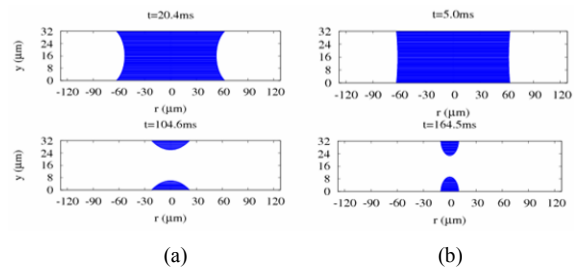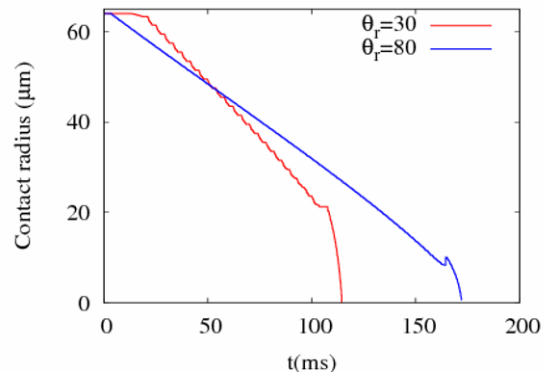orm with increasing plate gap. As a result, the evaporation rate decreases and the evaporation period increases with the plate gap, as plotted in Fig. 10. Although the gap decreases, the 2-dimensional prediction of evaporation period is much longer than the 1-dimensional prediction although using the small gap of $G = 16\,\mu m$. This means that 1-dimensional prediction is not easily applicable to the high-rate evaporation process, as the present case of $T_w = 90°C$.

3.4 Effect of the receding contact angle

Figs. 11 and 12 present the effect of receding contact angle on the temporal variations of an interface and liquid droplet radii. As the receding contact angle decreases, the interface deformation is pronounced as depicted in Fig. 11 and the con-

tact line pinning period increases as seen in Fig. 12. As a result, the evaporation rate increases as the contact angle decreases and the liquid droplet-air contact area increases.

4. Conclusions

Numerical simulations of droplet evaporation in the confined geometry between two circular plates, which is a well-defined and easily controllable evaporation process, were performed using a level-set method, which was extended to include the effect of evaporation at the liquid-gas interface and dynamic contact angles at the liquid-gas-solid contact line. The computations were used to validate the assumptions in the 1-dimensional theoretical analysis reported in the literature. The theoretical prediction showed a good agreement with the numerical results obtained by neglecting the transient and convection terms and assuming no heat transfer. When including the effects of convection and heat transfer, however, the theoretical prediction of evaporation time was much shorter than the numerical predictions. As the gap decreases, the 2-dimensional numerical prediction is closer to the 1-dimensional theoretical prediction, but the difference is not negligible even for the small gap. This means that the characteristics of flow, heat and mass transfer are not negligible across the film thickness normal to the plates for the case of the high-rate evaporation process. The evaporation rate was observed to increase as the receding contact angle decreased.

Acknowledgment

Nomenclature━━━━━━━━━━━━━━━━

c_f	: Specific heat of fluid
c_g	: Specific heat of gas
c_l	: Specific heat of liquid
D_g	: Diffusion coefficient of gas
$\hat{D}$	: Effective diffusion coefficient
F	: Fraction function
G	: Gap of two circular plates
h	: Grid spacing
h_{lg}	: Latent heat of vaporization
H	: Step function
k_f	: Thermal conductivity of fluid
k_g	: Thermal conductivity of gas
k_l	: Thermal conductivity of liquid
$\hat{k}$	: Effective thermal conductivity
$\dot{m}$	: Mass flux across the interface
M_a	: Molecular mass of air
M_v	: Molecular mass of vapor
$\mathbf{n}$	: Unit normal vector
p	: Pressure

$p_{v,sat}$	: Vapor saturation pressure
p_∞	: Atmospheric pressure
r, y	: Cylindrical coordinates
R	: Radius of liquid droplet
R_i	: Initial radius of liquid droplet
R_o	: Radius of circular plates
S	: Sign function
t	: Time
T	: Temperature
T_f	: Temperature of fluid
T_i	: Initial temperature
T_{int}	: Temperature at the liquid-gas interface
$\mathbf{u}$	: Flow velocity vector
$\mathbf{u}_f$	: Flow velocity vector of fluid
$\mathbf{u}_g$	: Flow velocity vector of gas
$\mathbf{u}_l$	: Flow velocity vector of liquid
$\mathbf{U}$	: Interface velocity vector
v_{lg}	: Difference between the liquid and gas specific volume
Y	: Vapor mass fraction
Y_{int}	: Vapor mass fraction at the interface
Y_o	: Vapor mass fraction at the right boundary
θ_a	: Advancing contact angle
θ_r	: Receding contact angle
κ	: Interface curvature
μ_g	: Dynamic viscosity of gas
μ_l	: Dynamic viscosity of liquid
$\hat{\mu}$	: Effective dynamic viscosity
ρ_f	: Density of fluid
ρ_g	: Density of gas
ρ_l	: Density of liquid
$\hat{\rho}$	: Effective density
σ	: Surface tension
τ_0	: Artificial time
τ_e	: Total evaporation time
ϕ	: Distance function from the liquid-gas interface
ξ	: Transformed coordinate

References

[1] T. Kawase, T. Shimoda, C. Newsome, H. Sirringhaus and R. H. Friend, Inkjet printing of polymer thin film transistors, *Thin Solid Films*, 438 (2003) 279-287.

[2] H. Koo, M. Chen and P. Pan, LCD-based color filter films fabricated by a pigment-based colorant photo resist inks and printing technology, *Thin Solid Films*, 515 (2006) 896-901.

[3] J. Berthier, *Microdrops and digital microfuidics*, 1st Ed., William Andrew (2008).

[4] A. F. Routh, Drying of thin colloidal films, *Reports on Progress in Physics*, 76 (2013) 046603.

[5] R. G. Picknett and R. Bexon, The evaporation of sessile or pendant drops in still air, *Interface J. of Colloid and Interface Science*, 61 (1977) 336-350.

[6] H. Y. Erbil, Evaporation of pure liquid sessile and spherical suspended drops: A review, *Adv. Colloid Interface Sci.*, 170 (2012) 67-86.

[7] F. Clément and J. Leng, Evaporation of liquids and solutions in confined geometry, *Langmuir*, 20 (2004) 6538-6541.

[8] J. Leng, Drying of a colloidal suspension in confined geometry, *Physical Review*, 82 (2010) 021405.

[9] L. Daubersies and J. B. Salmon, Evaporation of solutions and colloidal dispersion in confined droplets, *Physical Review E*, 84 (2011) 031406.

[10] H. Hu and R. G. Larson, Analysis of the microfluid flow in an evaporating sessile droplet, *Langmuir*, 21 (2005) 3963-3971.

[11] E. Widjaja and M. T. Harris, Numerical study of vapor phase-diffusion driven sessile drop evaporation, *Computers & Chemical Engineering*, 32 (2008) 2169-2178.

[12] O. E. Ruiz and W. Z. Black, Evaporation of water droplets placed on a heated horizontal surface, *J. of heat transfer*, 124 (5) (2002) 854-863.

[13] A. M. Briones, J. S. Ervin, S. A. Putnam, L. W. Byrd and L. Gschwender, Micrometer-sized water droplet impingement dynamics and evaporation on a flat dry surface, *Langmuir*, 26 (2010) 13272-13286.

[14] S. Tanguy, T. Ménard and A. Berlemont, A level-set method for vaporizing two-phase flows, *J. of Computational Physics*, 211 (2007) 837-853.

[15] G. Son, A level-set method for analysis of microdroplet evaporation on a heated surface, *J. of Mechanical Science and Technology*, 24 (2010) 991-997.

[16] G. Son, Numerical simulation of microdroplet impact and evaporation on a solid surface, *J. of Heat Transfer*, 134 (2012) 101502.

[17] G. Son and V. K. Dhir, A level set method for analysis of film boiling on an immersed solid surface, *Numerical Heat Transfer, Part B: Fundamentals*, 52 (2007) 153-177.

[18] J. Fukai, Y. Shiiba, T. Yamamoto, O Miyatake, O. Poulikakos, C. M. Megaridis and Z. Zhao, Wetting effects on the spreading of a liquid droplet colliding with a flat surface: Experiment and modelling, *Physics of Fluids*, 7 (1995) 236-247.

[19] T. F. Irvine and P. E. Liley, *Steam and gas tables with computer equations*, Academic Press (1984).

Hangjin Ban received a B.S. in Mechanical Engineering from Sogang University in 2014. He is a graduate student of Mechanical Engineering at Sogang University in Seoul, Korea. Ban's research interests are in the area of microfluidics and multiphase dynamics.

Gihun Son received his B.S. and M.S. in Mechanical Engineering from Seoul National University in 1986 and 1988, respectively, and his Ph.D. in Mechanical Engineering from UCLA in 1996. Dr. Son is currently a professor of Mechanical Engineering at Sogang University in Seoul, Korea. His research interests are in the areas of multiphase dynamics, heat transfer, and power system simulation.